Journal of Hydrology 517 (2014) 836–846

Contents lists available at ScienceDirect

Journal of Hydrology

journal homepage: www.elsevier.com/locate/jhydrol

Real-time multi-step-ahead water level forecasting by recurrent neural networks for urban flood control

Fi-John Chang [a,*], Pin-An Chen [a], Ying-Ray Lu [a], Eric Huang [b], Kai-Yao Chang [b]

[a] Department of Bioenvironmental Systems Engineering, National Taiwan University, Taipei 10617, Taiwan, ROC
[b] Hydraulic Engineering Office, Public Works Department, Taipei City Government, Taipei 11008, Taiwan, ROC

ARTICLE INFO

Article history:
Received 27 December 2013
Received in revised form 10 June 2014
Accepted 11 June 2014
Available online 20 June 2014
This manuscript was handled by Andras Bardossy, Editor-in-Chief, with the assistance of Purna Chandra Nayak, Associate Editor

Keywords:
Artificial neural networks (ANNs)
Nonlinear autoregressive network with exogenous inputs (NARX)
Gamma test
Flood forecast
Floodwater storage pond (FSP)
Urban flood control

SUMMARY

Urban flood control is a crucial task, which commonly faces fast rising peak flows resulting from urbanization. To mitigate future flood damages, it is imperative to construct an on-line accurate model to forecast inundation levels during flood periods. The Yu–Cheng Pumping Station located in Taipei City of Taiwan is selected as the study area. Firstly, historical hydrologic data are fully explored by statistical techniques to identify the time span of rainfall affecting the rise of the water level in the floodwater storage pond (FSP) at the pumping station. Secondly, effective factors (rainfall stations) that significantly affect the FSP water level are extracted by the Gamma test (GT). Thirdly, one static artificial neural network (ANN) (backpropagation neural network-BPNN) and two dynamic ANNs (Elman neural network-Elman NN; nonlinear autoregressive network with exogenous inputs-NARX network) are used to construct multi-step-ahead FSP water level forecast models through two scenarios, in which scenario I adopts rainfall and FSP water level data as model inputs while scenario II adopts only rainfall data as model inputs. The results demonstrate that the GT can efficiently identify the effective rainfall stations as important inputs to the three ANNs; the recurrent connections from the output layer (NARX network) impose more effects on the output than those of the hidden layer (Elman NN) do; and the NARX network performs the best in real-time forecasting. The NARX network produces coefficients of efficiency within 0.9–0.7 (scenario I) and 0.7–0.5 (scenario II) in the testing stages for 10–60-min-ahead forecasts accordingly. This study suggests that the proposed NARX models can be valuable and beneficial to the government authority for urban flood control.

1. Introduction

Urban flood control is a crucial and challenging task, particularly in developed cities. Urban floods are flashy in nature mainly due to severe thunderstorms and occur both on urbanized surfaces and in small urban creeks, which deliver mass water to cities. On account of more impervious areas resulting from the rapid urbanization in metropolitan areas, less water infiltration has resulted in an increase in the flow rate and the amount of surface runoff over the last decades. Taiwan is located in the northwestern Pacific Ocean where subtropical air currents frequently introduce typhoons and convective rains. The urban flood hydrographs in Taiwan typically have large peak flows and fast-rising limbs in a matter of minutes, which could cause serious disasters. For example, Typhoon Nari brought massive rainfalls at an astounding level of 500 mm/day on September 17th in 2001, which resulted in 27 deaths, inundations at some stations of the Taipei Metro System, and countless economic losses. The heavy rainfall event on June 12th in 2012 brought astonishing rainfalls with a cumulative amount of 54.1 mm/hr, which directly resulted in quick and wide surface flooding such that the transportation system collapsed in most of the southern Taipei City. It appears floods cannot be prevented, but planning emergency measures through flood management might mitigate disastrous consequences.

In response to the flood threat to residents and property, the Taipei City Government has long-term endeavored in developing flood control-related infrastructures, such as increasing levee heights and enhancing sewerage systems, and urban inundations have been significantly mitigated and controlled in recent years. As a result, the main threat to the city turns out to be the floodwater inside the levee system. A surface inundation will inevitably take place if surface runoff exceeds the capacity of a storm drainage system. To tackle this problem, pumping stations play an important role in flood mitigation at metropolitan areas and are principal hydraulic facilities built to manage internal stormwater

* Corresponding author. Tel.: +886 2 23639461; fax: +886 2 23635854.
E-mail address: changfj@ntu.edu.tw (F.-J. Chang).

http://dx.doi.org/10.1016/j.jhydrol.2014.06.013
0022-1694/

flows at places under the condition that gravity drainage cannot be achieved. The operation of a pumping station highly depends on the water level information of its floodwater storage pond (FSP). Within the catchment of a pumping station, surface runoff will drain to its FSP for storage and subsequent disposal through gravity drainage. When the water level of the FSP reaches the start level of duty pumps, the pumps will be activated according to operation rules for discharging the stored floodwater into the nearby river. For floodwater control management during heavy rainfall or typhoon events, it is imperative to construct an efficient and accurate model to forecast many step-ahead FSP water levels by utilizing the information of the current FSP water level and the rainfall measured at the neighboring rainfall gauging stations of the pumping station. The proposed model is expected to provide sufficient response time for warming up the pumps in advance for enhancing secure pumping operations and urban flood control management.

Artificial neural networks (ANNs) possess the ability to approximate nonlinear functions, and therefore become useful tools for handling water resources problems such as rainfall forecasting (Hung et al., 2009; Nasseri et al., 2008), stream flow forecasting (Akhtar et al., 2009; Besaw et al., 2010; Chen et al., 2013; Nayak, et al., 2013; Sudheer et al., 2008; Toth, 2009; Sahoo et al., 2009), water level forecasting (Alvisi et al., 2006; Makarynskyy et al., 2004; Ali Ghorbani et al., 2010), and applications in urban drainage systems (Bruen and Yang, 2006; Loke et al., 1997; Chang et al., 2008; Chiang et al., 2010). Signal delays play an important role in neurobiological information processing. This concept has led to the development of dynamic neural networks. Recurrent neural networks (RNNs) that facilitate time delay units through feedback connections are computationally more powerful and biologically more plausible than other adaptive approaches such as feedforward networks, and thus have attracted much attention for years (Assaad et al., 2005; Chang et al., 2012; Coulibaly and Baldwin, 2005; Coulibaly and Evora, 2007; Ma et al., 2008; Muluye, 2011; Serpen and Xu, 2003). RNNs can be trained to learn sequential or time-varying patterns and are considered very effective in modeling the dynamics of complex hydrological processes with accurate forecasts; consequently their capability in modeling multi-step-ahead forecasts in highly variable time series is investigated. As known, multi-step-ahead forecasting is much more complex to deal with than one-step-ahead forecasting (Sorjamaa et al., 2007), and we believe ANNs, especially recurrent ones, can play an important role in tackling these complex tasks.

The greatest success in flood forecasting is commonly achieved on large rivers. Nevertheless, flash urban floods associated with heavy thunderstorms in cities are often very uncertain and are more difficult to predict due to complex dynamic phenomena involved. Many studies demonstrated the predictability of streamflow through soft computation methods (Nayak, et al., 2004; Maity and Kumar, 2008) while only few papers investigated the prediction performance of inundation and/or sewerage systems in urban areas (Chiang et al., 2010). In this study, we intend to investigate the reliability and accuracy of short-term (10–60-min) forecast models for the floodwater storage pond (FSP) of a sewer-pumping system in Taipei City, Taiwan. The multi-step-ahead FSP water level forecast models for flood pumping control during heavy rainfall and/or typhoon events are tailored made through a static ANN (the back-propagation neural network-BPNN) and two dynamic ANNs (the Elman NN; the nonlinear autoregressive with eXogenous input-NARX network). Consequently, the comparison results of these three ANN models are evaluated for the effectiveness of recurrent connections. The forecasting system is designed to anticipate the occurrence of flooding and to take measures necessary to reduce flood-induced losses. The study will give a boost to the efforts for urban flood disaster management and strengthen the Taipei City Government with more proactive disaster preparedness.

2. Methodology

In this study, various ANNs are used to make water level forecasts for representing the behavior of the rainfall-sewer flow processes in storm events. Flood levels can be forecasted on the basis of (a) rainfall data; (b) previous water levels; and (c) a combination of both data sets. We adopt three ANNs coupled with statistical techniques to construct real time multi-step-ahead FSP forecast models. The implementation procedure is shown in Fig. 1. The time span of rainfall affecting the rise of FSP water level is first identified by the correlation analysis. Next the Gamma test (GT) is applied to extracting effective rainfall factors from all possible rainfall-related input combinations. One static (BPNN) and two dynamic (Elman NN and NARX network) neural networks are proposed to construct multi-step-ahead FSP water level forecasts for two scenarios (w/ and w/o current FSP water level information). Finally, these constructed ANN models are evaluated by performance criteria. The methods used in this study are briefly addressed as follows.

2.1. Gamma test (GT)

The GT, presented by Agalbjorn et al. (1997) and Koncar (1997), is a data analysis technique for assessing the extent to which a

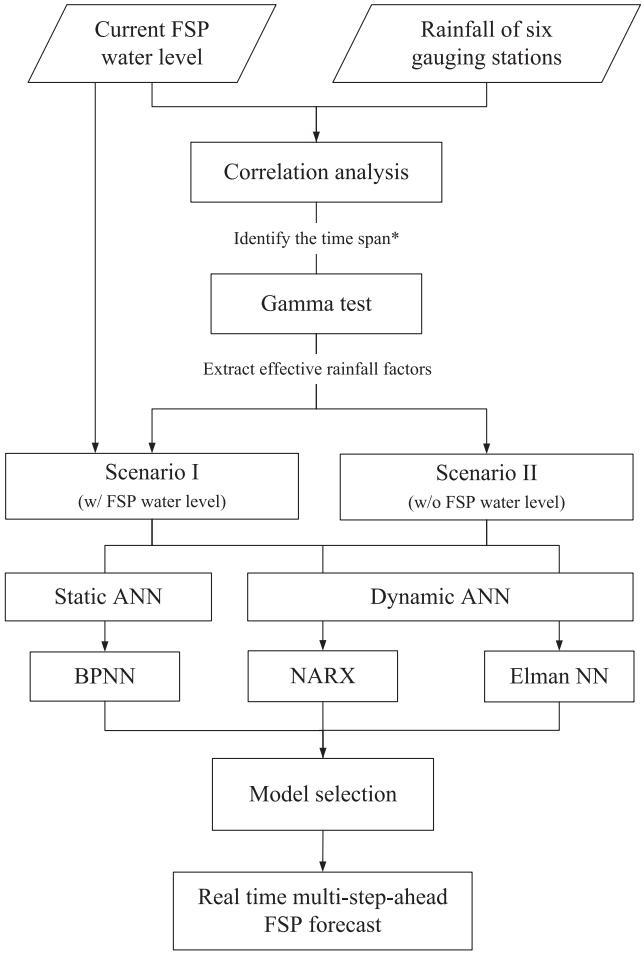

Fig. 1. Architecture of the study flow. *Time span of rainfall affecting the rise of FSP (floodwater storage pond) water level.

given set of M data points can be modeled by an unknown smooth non-linear function. The Gamma statistic (Γ) is an estimate of the model output's variance that cannot be accounted for through a smooth data model. Performing a single GT is a fast procedure, which can provide the noise estimate (Γ value) for each subset of input variables. When the subset produces its associated Γ value closest to zero, it can be considered as "the best combination" of input variables. Several studies discussed about the GT theory and its applications in time series forecasting (Durrant, 2001; Tsui et al., 2002). Lately, research findings indicate it is suitable and effective to combine ANNs with the GT for identifying non-trivial input variables and thus reduces the input dimensions as well as produces precise outputs of ANNs (Chang et al., 2013; Moghaddamnia et al., 2009; Noori et al., 2011). Therefore, ANNs combine the GT to determine the representative rainfall gauging stations affecting the FP water level in the study catchment.

2.2. Backpropagation neural network (BPNN)

The BPNN is one of the most popular ANNs (Rumelhart, 1986). It belongs to a typical three-layered static feedforward neural network, which is comprised of multiple elements including nodes and weight connections (**W** and **V**) that link nodes. The network is divided into an input layer, a hidden layer and an output layer. Fig. 2(a) shows the structure of BPNN. In this study, BPNN is trained by the Levenberg–Marquardt back propagation algorithm based on the model output ($z(t+N)$) and observed data ($d(t+N)$), and the transfer functions of hidden and output layers are of sigmoid and linear types, respectively.

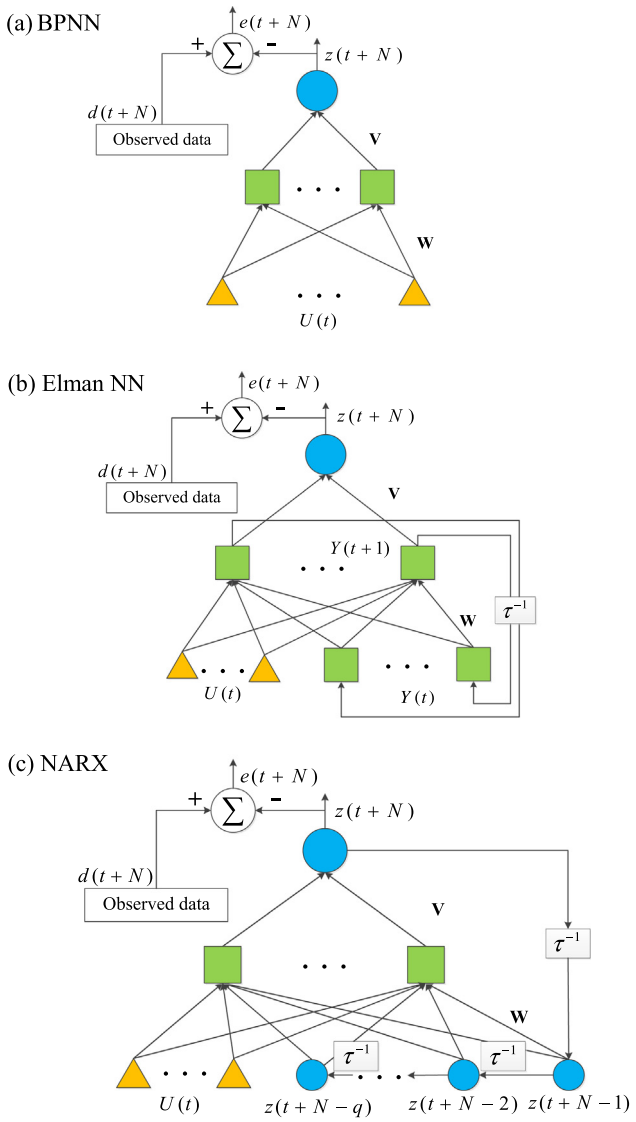

Fig. 2. Architectures of (a) the BPNN, (b) the Elman NN, and (c) the NARX network.

2.3. Elman neural network (Elman NN)

The Elman NN (Elman, 1990) is a three-layer RNN with internal time-delay feedback connections in the hidden layer. Each input neuron is connected to a hidden neuron, where each hidden neuron has its corresponding time-delay unit. The structure of the Elman NN is shown in Fig. 2(b). Basically, a recurrent connection allows its time-delay unit to store the information of this hidden neuron as an additional input to all hidden neurons at the next time-step. Therefore, the Elman NN has an inherent dynamic memory given by the recurrent connections of the time-delay units, and its output depends not only on the current input information but also on the previous states of the network. In this study, the Elman NN is also trained by the Levenberg–Marquardt back propagation algorithm, and the transfer functions of hidden and output layers are of sigmoid and linear types, respectively.

2.4. Nonlinear autoregressive with eXogenous input (NARX) network

The NARX network is a recurrent network, which is suitable for time series prediction (Chang et al., 2013; Jiang and Song, 2011; Lin et al., 1998; Menezes Jr. and Barreto, 2008, Shen and Chang, 2013). Fig. 2(c) shows the architecture of the NARX network used in this study. The NARX network consists of three layers and produces recurrent connections from the outputs, which may delay several unit times to form new inputs. Therefore, this nonlinear system for N-step-ahead forecasting ($N \geqslant 1$) can be mathematically represented by the following equation:

$$z(t+N) = f[z(t+N-1), \ldots, z(t+N-q);\ U(t)] \quad (1)$$

where $U(t)$ and $z(t+N)$ denote the input vector and output value at the time step t, respectively. $f(\cdot)$ is the nonlinear function, and q is the output-memory order. There are two input regressors: the regressor $z(t+N-i)$ (i is 1 to q) plays the role of an autoregressive model while the other one, $U(t)$, plays the role of an implicit exogenous variable in time series.

There are two ways to train the NARX network. The first mode is the Series–parallel (SP) mode, where the output's regressor in the input layer is formed only by the target (actual) values of the system, $d(t)$.

$$z(t+N) = f[d(t+N-1), \ldots, d(t+N-q);\ U(t)] \quad (2)$$

The other alternative is the Parallel (P) mode, where estimated outputs are fed back into the output's regressor in the input layer, which can also be mathematically represented as Eq. (1). In practice, when forecasts are conducted for more than two-step-ahead ($N > 1$), the q antecedent actual values ($d(t+N-1)$, $d(t+N-2)$, $\ldots$, $z(t+N-q)$) are future data that cannot be obtained at current time. Bearing this consideration, the NARX network is trained in P mode with imperfect information and retains similar characteristics of input–output patterns in the testing stages, and therefore the constructed NARX network can maintain similar capability of real time multi-step-ahead forecasts in both training and testing stages. In this study, the NARX network is also trained by the Levenberg–Marquardt back propagation algorithm, and the transfer functions of hidden and output layers are of sigmoid and linear type, respectively. Despite this important property

(recurrent connection) of the NARX network, its feasibility as a nonlinear tool for time series modeling and forecasting has not been fully explored yet.

3. Applications

3.1. Study area and dataset

Taiwan, an island located in the subtropical zone of the North Pacific Ocean, is covered with mountainous terrains and steep landforms. Taipei City, situated in the Taipei Basin of northern Taiwan, is surrounded by the Danshui River whose narrow estuary makes it difficult to discharge water effectively from the city. Consequently, the high levees along the Danshui River have been built to prevent outer flood into the city with a return period of two-hundred-year flood protection standard. Typhoons and/or heavy rainfall events are usually coupled with intensive rainfalls and thus easily cause urban flooding within a few hours, even within a few minutes, in Taipei City. Because of the high levees, the main threat to the city now turns out to be the floodwater inside the levee system. Therefore, pumping stations play an important role in managing internal stormwater flows for urban flood control. The Yu–Cheng catchment, located in southeastern Taipei, is selected as the study area (Fig. 3). There are six rainfall gauging stations (R1–R6, denoted as red dots in Fig. 3). Although station R2 is out of the catchment, it still belongs to a sewerage system that diverts floodwater to the Yu–Cheng pumping station and the Keelung River. There also exist a number of water level gauging stations in this study catchment. However, the malfunctions of water level gauges caused by their collisions with unknown objects and siltation in sewerage systems raise the difficulty in the maintenance of water level gauges and their online monitoring. The water level data collected from the sewerage system are neither stable nor accurate, which means the FSP water level forecast models for the Yu–Cheng Pumping Station would mostly rely on the rainfall information retrieved from its neighboring rainfall gauging stations.

The Yu–Cheng catchment occupies an area of about 1627 ha and owns the biggest drainage system in Taipei City. The Yu–Cheng Pumping Station was built in 1987 to drain or pump the internal stormwater flows into the Keelung River, a chief tributary of the Danshui River, and it was considered the most advanced and the largest pumping station in Asia in the 1980s. The pumping station is currently equipped with 11 pumps reaching a total pumping capacity of 234.1 cms, and the operation of the pumping station highly depends on the FSP water level information. If the FSP water level rises up to the warning level (1.8 m) during heavy rainfall or typhoon events, pumps are activated with a 3-min warm up. Then stormwater starts to be pumped from the FSP into the Keelung River when the FSP water level reaches the start level (2.2 m). The start level is the lowest water level designed for the start of stormwater pumping as well as for the prevention against the idle running of pumps to avoid pump damage. These 11 pump units operate independently and maintain a sequential operation according to the laddered FSP water levels during typhoon or heavy rainfall periods. This means the pumping operation begins with one pump unit, and only one pump unit, instead of all remaining pump units, will join the operation at a time if the next higher rung of the laddered water levels is reached. On the contrary, running pumps will be shut down sequentially as the FSP water level decreases to the next lower rung. The operational procedure of the Yu–Cheng Pumping Station is quite different from those of Hong Kong, Tokyo or Singapore, where all the pump units are activated at the beginning if the FSP water level exceeds the start level, then the pump units stop running as the FSP water level drops to the stop level (DSD, 2000; PUB, 2013; Tamoto et al., 2008). It suggests that the pumping operation in Taipei City is much more sensitive to the fluctuation of FSP water level than those of big cities in Monsoon Asia.

Data of FSP water levels and rainfall at stations R1–R6 were collected with a temporal resolution of 10 min from 13 typhoon

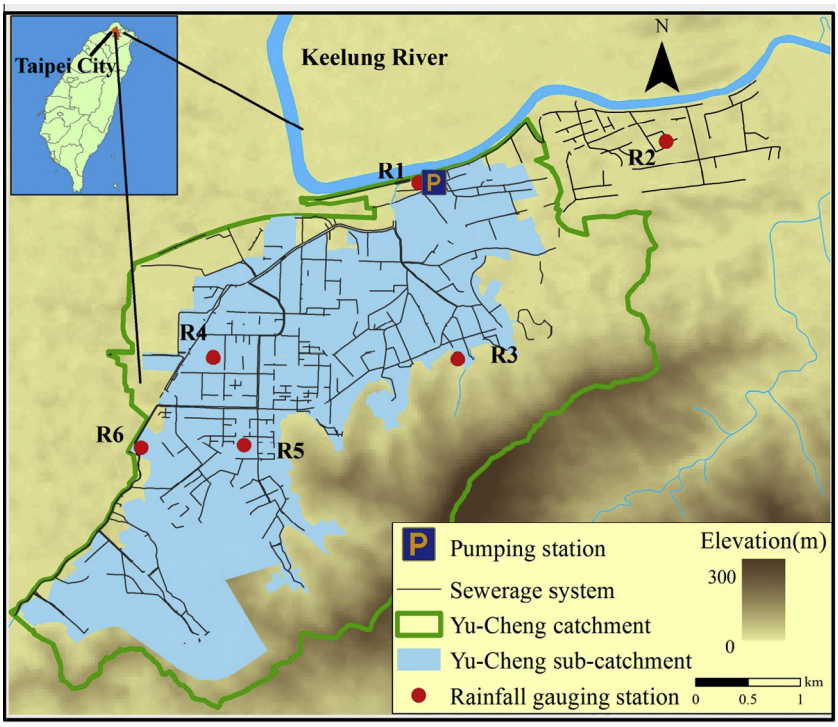

Fig. 3. Location of the Yu–Cheng catchment and rainfall gauging stations.

and heavy rainfall events during 2004 and 2013. A total of 1985 datasets are used for constructing forecast models in this study, and the numbers of datasets allocated into training, validation and testing stages are 826 (from 6 events), 651 (from 3 events) and 508 (from 4 events) accordingly. Such allocation is made to maintain similar statistic characteristics in these three datasets in consideration of the summary statistics of the 13 events shown in Table 1. In addition, the weighted average rainfall (R_{avg}) over the Yu–Cheng catchment is computed by the Thiessen polygon method and is also considered as a potential input to the forecast models. Furthermore, because the original FSP water level is indeed affected by the operation of pumping units. The original FSP water levels were recovered prior to model construction according to a recovery equation (provided by the Taipei City Government) that involves pumping capacity and pumping-affected area. The summary statistics for FSP water levels and rainfall datasets are presented in Table 1.

3.2. Identification of the time span of rainfall affecting the rise of the FSP water level

For constructing a rainfall-sewer flow model, the first step is to identify the temporal impacts of rainfall on the rise of FSP water level. In this study, the Pearson's correlation coefficient is applied to learning the linear relationship and the recognition of the highest correlations between FSP water level and rainfall at different time lags for each station (R1–R6) as well as the weighted average rainfall (R_{avg}) over the Yu–Cheng catchment. The results shown in Fig. 4 indicate that it consistently takes about 40 min for rainfall at stations R1–R6 to cause an increase in the FSP water level, similarly for the R_{avg}. It is worthy to note that, in contrast to the river channel, a sewerage system can be implicitly considered as a small-scale volume control system on account of the relatively small catchment with which the system was associated. The variation of the FSP water level is mainly affected by the rainfall aggregated within a short period of time in the catchment. As a result, the time span of rainfall affecting the rise of FSP water level at the Yu–Cheng Pumping Station is set as 40 min. It is noted that "time span" is used in this study while "concentration time" is usually used in river channel studies.

3.3. Extraction of effective rainfall factors

The Pearson's correlation coefficients between the FSP water level and rainfall at gauging stations R1–R6 as well as R_{avg} are not very high but quite similar (ranging from 0.41 to 0.63), which could be due to the lumped effect of rainfall falling to the catchment and the complex interactions between rainfall and sewer flow. In order to identify effective rainfall stations that significantly affect the fluctuations of FSP water level for modeling purpose, the GT is implemented in this study. That is to say, rainfall-related inputs to the estimation models of FSP water level is determined by the GT.

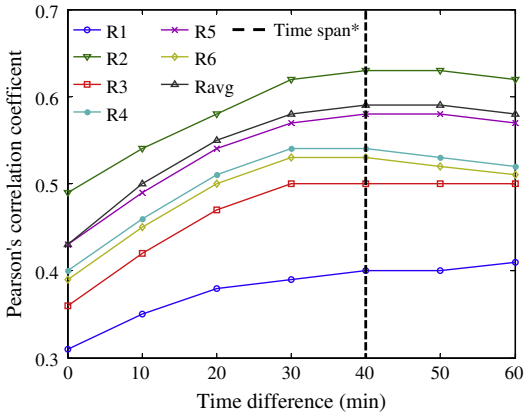

Fig. 4. Correlation analysis between FSP water levels and rainfall gauging stations in different time steps. *Time span of rainfall affecting the rise of FSP water level.

3.4. Model construction

In this study, one- to six-step-ahead FSP water level forecast models during heavy rainfall and typhoon events for the Yu–Cheng Pumping Station are constructed through the BPNN, the Elman NN and the NARX network based on the inputs determined by the GT. The practical meaning and contribution of three forecast models will be surveyed under two scenarios: (1) the information of current FSP water level is available (denoted as scenario I hereinafter); (2) the information of current FSP water level is not available (denoted as scenario II hereinafter). During model construction and selection, the structures of the three types of NNs (BPNN, Elman NN and NARX network) are evaluated and identified mainly based on the summary statistics of their performances in three independent datasets (i.e., training, validation and testing datasets). For each type of NNs, various model structures associated with different node numbers are constructed and evaluated to obtain their training performances. When the training process is completed, several candidate NNs that have different structures are obtained. Then the trained NN that produces the best performance in the validation stage is selected as the final model to be

Table 1
Summary statistics for FSP water levels (m) and the peaks of average rainfall (mm/10 min).

Event configuration	Model stage	Number of data	Peak of average rainfall intensity (mm/10 min)	Max FSP water level (m)	Mean FSP water level (m)	Standard deviation (m)
1	Training	826	15.3	5.68	3.12	1.04
2			8.43	3.08	2.50	0.24
3			8.03	2.73	2.25	0.28
4			3.37	2.40	2.07	0.14
5			2.26	2.41	2.13	0.09
6			5.17	2.57	1.79	0.37
7	Validation	651	11.0	3.69	2.23	0.48
8			10.1	2.68	2.05	0.39
9			5.91	2.85	2.07	0.31
10	Testing	508	5.47	2.84	2.17	0.18
11			6.99	2.69	2.25	0.19
12			4.92	2.50	2.08	0.26
13			12.4	4.59	2.57	0.55

further tested by the testing dataset for evaluating its reliability. This model selection strategy is applied to the BPNN, the Elman NN and the NARX network, respectively.

The applicability and reliability of these three constructed forecast models at different forecasting steps are evaluated by the root mean square error (RMSE), correlation coefficient (CC) and coefficient of efficiency (Nash Efficiency or CE) (Nash and Sutcliffe, 1970), as shown below.

$$\mathrm{RMSE} = \sqrt{\frac{\sum_{i=1}^{n}(\hat{H}_i - H_i)^2}{n}} \tag{3}$$

$$\mathrm{CC} = \frac{\sum_{i=1}^{n}(\hat{H}_i - \bar{\hat{H}})(H_i - \bar{H})}{\sqrt{\sum_{i=1}^{n}(\hat{H}_i - \bar{\hat{H}})^2 \sum_{i=1}^{n}(H_i - \bar{H})^2}} \tag{4}$$

$$\mathrm{CE} = 1 - \frac{\sum_{i=1}^{n}(\hat{H}_i - H_i)^2}{\sum_{i=1}^{n}(H_i - \bar{H})^2} \tag{5}$$

where $\hat{H}_i$ and H_i are the forecasted and observed FSP water levels of the ith data, respectively. $\bar{\hat{H}}$ and $\bar{H}$ are the average forecasted and observed FSP water levels, respectively. And n is the number of data points.

4. Results and discussion

This section presents the selection result of effective rainfall factors and the forecast performance of the static (BPNN) and dynamic (Elman NN and NARX) neural networks in two scenarios (w/ and w/o current FSP water level information). The results and discussion are addressed in details, which are shown as follows.

4.1. Identification of effective rainfall stations

For extracting effective rainfall factors, data of the antecedent 40-min rainfall collected at six gauging stations together with the average rainfall (R1($t-4$)–R6($t-4$), $R_{avg}(t-4)$) are first scaled to $[-1,1]$. Then a total of 127 (2^7-1) Γ values corresponding to all possible rainfall-related input combinations are calculated through the GT. The produced Γ values are next sorted in an ascending order, in which Γ values smaller than the 10th percentile ($\Gamma_{10}=0.10$) are classified as the best group ($F_{\Gamma\leqslant\Gamma_{10}}$), whereas those bigger than the 90th percentile ($\Gamma_{90}=0.17$) are classified as the worst group ($F_{\Gamma\geqslant\Gamma_{90}}$). Fig. 5 shows the result of the GT, where blue bars represent the occurrence frequency of factors in the best group ($F_{\Gamma\leqslant\Gamma_{10}}$) while orange bars represent the occurrence frequency of factors in the worst group ($F_{\Gamma\geqslant\Gamma_{90}}$), and factor scores calculated by Eq. (6) for each rainfall factors are drawn into a green dotted line.

$$\text{factor score} = 1 - \frac{F_{\Gamma\geqslant\Gamma_{90}}}{F_{\Gamma\leqslant\Gamma_{10}}} \tag{6}$$

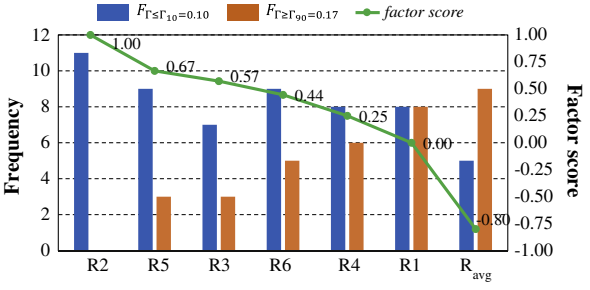

Fig. 5. Determination of effective rainfall stations by the GT results.

where the factor score ranges from $-\infty$ to 1.

Therefore, effective rainfall factors can be identified as those factors that are associated with higher factor scores, and the threshold of the factor score is set as 0.5 in this study. Consequently, stations R2, R3 and R5 are identified as the effective rainfall factors to be used in the forecast models.

4.2. Performance of FSP water level forecasts in scenario I: Current FSP water level is available

In scenario I, data of the current FSP water level and rainfall of R2, R3 and R5 are utilized to construct 10–60-min-ahead (N = 1–6) FSP water level forecast models through three ANNs. The input–output patterns of three ANN models can be represented as follows:

$$\hat{WL}_{\mathrm{FSP}}(t+N) = f[WL_{\mathrm{FSP}}(t),\ \mathrm{R2}(t+N-4),\ \mathrm{R3}(t+N-4),\ \mathrm{R5}(t+N-4)]$$
$$N \in 1\text{–}4(10\ \mathrm{min}) \tag{7}$$

$$\hat{WL}_{\mathrm{FSP}}(t+N) = f[WL_{\mathrm{FSP}}(t),\ \mathrm{R2}(t),\ \mathrm{R3}(t),\ \mathrm{R5}(t)]$$
$$N \in 5\text{–}6(10\ \mathrm{min}) \tag{8}$$

where $\hat{WL}_{\mathrm{FSP}}(t+N)$ is the forecast at a lead time of N (10-min unit).

After implementing trial-and-error procedures for model configuration based on the training and validation data sets, the output-memory order q for NARX networks is 1 and all the three models are configured to have only one hidden layer with 2–4 nodes for different forecasting steps. Summarized results are presented in Table 2. Results indicate that the three comparative models perform rather consistently in the training and validation stages while both dynamic neural networks (the Elman NN and NARX network) perform better than the static one (the BPNN) in the testing stages. Besides, the NARX network outperforms the Elman NN as the forecasting step exceeds four, and it even produces a high CE value (close to 0.7) as the forecasting step reaches six (60-min-ahead forecast).

The 612 heavy rainfall event (12.4 mm/10-min; 54.1 mm/h) with the highest peak FSP water level above 4.5 m is selected to illustrate the hydrographs of observed versus 20, 50 and 60-min-ahead forecasted FSP water levels in the testing stages of three models (Fig. 6). And during the peak flow period (about 10 h) of this event, 6 up to 11 pumping units were operated. Results show that the Elman NN produces the best performance for 20-min-ahead forecasting because its over-estimation between 10 and 20 time steps is comparatively less serious. However, the NARX network can significantly mitigate the time-lag problem at the peak value and well forecast the 50 and 60-min-ahead FSP water levels, whereas the other two comparative models not only have significant time-lag phenomena but fail to well forecast 50 and 60-min-ahead water levels, in which fluctuations occur near peak values.

Fig 7(a) shows the CE of 10–60-min-ahead forecasts in the testing stages of three models in scenario I. The three network models perform equally well for one- to three-step-ahead forecasting, whereas significant differences among their performances are found as the forecasting time step exceeds four (40 min). The reason is that the time span of rainfall affecting the rise of the FSP water level is 40 min such that the rainfall-water level processes at 1–4 time steps could be suitably presented by rainfall input data and FSP water level output data (Eq. (7)). In addition to the fact that the persistence of FSP water level decreases as the time step increases, the time lag of rainfall becomes significant as the forecasting time step exceeds four. As a result, both conditions would cause a reduction in forecasting accuracy. It clearly indicates that the NARX networks produce much higher CE values than the other

Table 2
Model performance of one- to six-step-ahead forecast for FSP water levels in scenario I.

Time step	Number of nodes	Model stage	BPNN			Elman NN			NARX		
			RMSE (m)	CC	CE	RMSE (m)	CC	CE	RMSE (m)	CC	CE
$t+1$	2	Training	0.07	0.99	0.99	0.07	0.99	0.99	0.07	0.99	0.99
		Validation	0.07	0.98	0.96	0.07	0.98	0.97	0.07	0.98	0.96
		Testing	0.10	0.96	0.92	0.09	0.96	0.93	0.09	0.97	0.93
$t+2$	2	Training	0.12	0.98	0.96	0.11	0.98	0.97	0.11	0.98	0.96
		Validation	0.12	0.94	0.89	0.10	0.96	0.91	0.12	0.94	0.89
		Testing	0.17	0.90	0.77	0.15	0.91	0.82	0.16	0.91	0.79
$t+3$	2	Training	0.14	0.97	0.95	0.14	0.97	0.95	0.14	0.97	0.95
		Validation	0.14	0.91	0.83	0.14	0.92	0.84	0.15	0.90	0.81
		Testing	0.18	0.89	0.71	0.18	0.88	0.72	0.18	0.88	0.72
$t+4$	2	Training	0.15	0.97	0.94	0.15	0.97	0.94	0.18	0.96	0.91
		Validation	0.16	0.88	0.78	0.17	0.88	0.77	0.20	0.82	0.65
		Testing	0.21	0.87	0.62	0.19	0.88	0.67	0.18	0.86	0.70
$t+5$	3	Training	0.20	0.95	0.89	0.19	0.95	0.90	0.17	0.96	0.92
		Validation	0.19	0.85	0.70	0.17	0.87	0.75	0.19	0.85	0.70
		Testing	0.22	0.82	0.57	0.20	0.83	0.65	0.19	0.87	0.69
$t+6$	4	Training	0.24	0.92	0.84	0.22	0.94	0.87	0.16	0.96	0.93
		Validation	0.19	0.85	0.70	0.19	0.84	0.69	0.22	0.78	0.58
		Testing	0.23	0.77	0.52	0.22	0.79	0.58	0.19	0.88	0.67

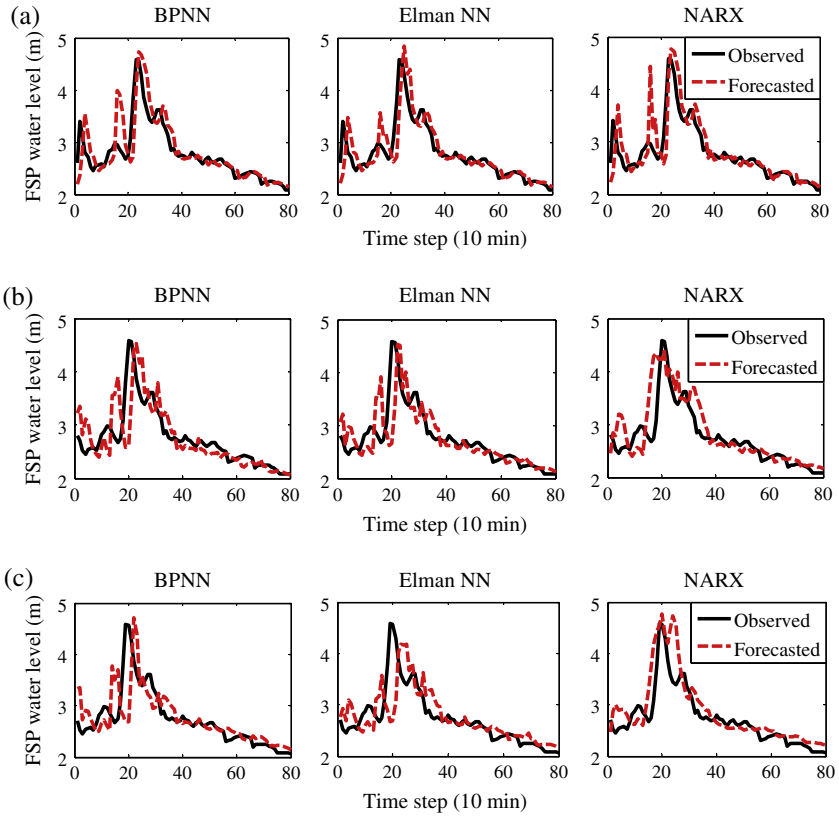

Fig. 6. (a) 20, (b) 50 and (c) 60-min-ahead forecasts of the 612 heavy rainfall event for scenario I with respect to the BPNN, Elman NN and NARX network.

two models for four to six-step-ahead forecasting, whereas the Elman NNs perform slightly better than the BPNNs.

Finally, the relationship between forecast errors (RMSE) and forecasting steps of these three models is presented in Fig. 7(b). The RMSE trend of the NARX network model increases gradually as the forecasting step increases, and it becomes flat after three forecasting steps. Nevertheless the RMSE trends of the BPNN and the Elman NN models significantly increase as the forecasting step increases, and they have steeper slopes than that of the NARX after three forecasting steps. The results provide evidence that with the feedbacks of imperfect outputs representing the information closest to the forecasting horizon to the input layer, the NARX network can effectively adopt extra information to promote the accuracy and reliability of multi-step-ahead FSP water level forecasts.

4.3. Performance of FSP water level forecasts in Scenario II: Current FSP water level is unavailable

In the flood control centre of the Taipei City Government, the datasets of the current FSP water level at sixty-five pumping

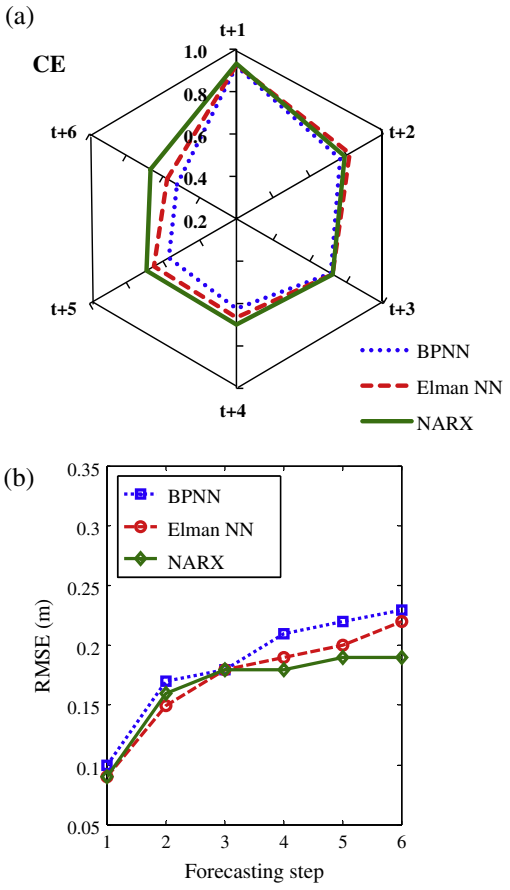

Fig. 7. (a) CE of 10- to 60-min-ahead forecasts and (b) relationship between FSP water level forecast errors (RMSE) and forecasting steps with respect to three forecast models in the testing stages for scenario I.

stations during typhoon events are transmitted only through two channels of radio waves, and thus the backend system of the flood control centre may not successfully receive the current FSP water level information every ten minutes. Furthermore, the preliminary correlation analysis results indicate the time span between the FSP water level and rainfall over the study catchment is about 40 min. An alternative to the forecast model of scenario I is considered essential for auxiliary purposes. In this scenario (II), FSP water level forecast models are constructed based only on the rainfall of R2, R3 and R5 to prevent any possible delay in the receipt of the current FSP water level due to the unstable frequency of data transmission. The input–output patterns of three ANN models can be represented as follows:

$$W\hat{L}_{FSP}(t+N) = f[\mathrm{R2}(t+N-4),\ \mathrm{R3}(t+N-4),\ \mathrm{R5}(t+N-4)] \quad N \in 1\text{—}4(10\ \mathrm{min}) \tag{9}$$

$$W\hat{L}_{FSP}(t+N) = f[\mathrm{R2}(t),\ \mathrm{R3}(t),\ \mathrm{R5}(t)] \quad N \in 5\text{—}6(10\mathrm{min}) \tag{10}$$

where $W\hat{L}_{FSP}(t+N)$ is the forecast at a lead time of N (10-min unit).

After implementing trial-and-error procedures for model configuration based on the training and validation data sets, the output-memory order q for NARX networks is 1 and all the three models are configured to have only one hidden layer with 2–4 nodes for different forecasting steps. Summarized results are presented in Table 3. Results indicate that the NARX networks significantly outperform the other two network models in terms of lower RMSE and higher CC and CE values in all three stages (training, validation and testing) for one- to six-step-ahead forecasts. It is noted that the performance of three ANN models in scenario II is not as good as that of scenario I. The reason is that only rainfall information is utilized as model inputs in scenario II, while another important factor, i.e., the persistent effect (auto-regression) of the FSP water level, is not considered (or unavailable) in this circumstance. Under such condition, the NARX network equipped with recurrent connections from imperfect outputs can produce much more satisfactory results than those of the Elman NN and the BPNN.

Similar to that of scenario I, an analysis is conducted on the 612 heavy rainfall event for scenario II. The rainfall input datasets from three gauging stations and 50-min-ahead forecasts are illustrated in Fig. 8. It demonstrates that the NARX network can well forecast the 50-min-ahead FSP water level and maintain the water level trail with less fluctuation than the BPNN and the Elman NN. The strong fluctuations occurring in the hydrographs associated with the BPNN and the Elman NN are mainly because these two models are driven only by the rainfall-related inputs that originally bear high variations, whereas the NARX network facilitates extra input information from the previous forecasted FSP water level to smooth the fluctuations of the forecasted hydrograph.

Fig 9(a) shows the CE of 10–60-min-ahead forecasts in the testing stages of three network models in scenario II. It clearly indicates that the NARX networks produce much higher CE values than the other two network models, while the Elman NNs perform even worse than the BPNNs, which implies the recurrent connections from the hidden layer of each Elman NNs magnify the highly variable rainfall information and thus do not increase the reliability of the Elman NNs.

Fig 9(b) illustrates the relationship between forecast errors (RMSE) and forecasting steps of these three models. The results show that the NARX network produces much lower RMSE values than the other two models for one- to six-step-ahead forecasting, and the RMSE values of three models are relatively consistent (flat) for one- to four-step-ahead forecasting. For the NARX network, the RMSE value is the lowest at the 4th forecasting step and start fast rising afterward. This is mainly because only current rainfall information is available as the forecasting step increases to five and six steps, which significantly causes the degradation of model performance at the 5th and 6th forecasting steps. This phenomenon is consistent with the 40-min time span of rainfall affecting the rise of the FSP water level, which is determined by the correlation analysis addressed in Section 3.2.

In brief, the NARX network implemented without the input of the current FSP water level information can still provide reasonable and reliable multi-step-ahead FSP water level forecasts, and therefore this model can be adopted for auxiliary purposes.

4.4. Summary of forecast performance

We explore the explanatory power in multi-step-ahead forecasting for FSP water levels through one static neural network (BPNN) and two dynamic neural networks (NARX network and Elmann NN). Results of scenario I demonstrate that the static network is inferior to the dynamic ones because the inputs of the static network depend solely on observed data, whereas those of the dynamic networks incorporate observed data with time delay units through recurrent connections either from the output layer (NARX network) or from the hidden layer (Elman NN), which makes significant contribution to the forecast values.

We further explore the ability of these two recurrent neural networks (NARX network and Elman NN) to solve the problem of long-term dependencies in a time series. We find that although the NARX network may not completely circumvent this problem, it can much effectively discover the long-term dependencies

Table 3
Model performance of one- to six-step-ahead forecast for FSP water levels in scenario II.

Time step	Number of nodes	Model stage	BPNN			Elman NN			NARX		
			RMSE (m)	CC	CE	RMSE (m)	CC	CE	RMSE (m)	CC	CE
$t+1$	3	Training	0.44	0.71	0.49	0.39	0.78	0.59	0.27	0.90	0.81
		Validation	0.35	0.46	0.01	0.33	0.42	0.13	0.31	0.56	0.25
		Testing	0.26	0.68	0.44	0.29	0.62	0.30	0.21	0.81	0.63
$t+2$	2	Training	0.48	0.74	0.39	0.39	0.78	0.59	0.27	0.90	0.81
		Validation	0.34	0.39	0.07	0.32	0.44	0.15	0.29	0.61	0.29
		Testing	0.26	0.66	0.43	0.27	0.66	0.37	0.20	0.84	0.67
$t+3$	2	Training	0.42	0.75	0.53	0.38	0.79	0.60	0.24	0.92	0.84
		Validation	0.33	0.44	0.06	0.32	0.43	0.13	0.31	0.62	0.21
		Testing	0.26	0.66	0.41	0.28	0.65	0.34	0.21	0.80	0.64
$t+4$	2	Training	0.47	0.74	0.40	0.39	0.78	0.60	0.25	0.91	0.83
		Validation	0.32	0.42	0.14	0.32	0.42	0.12	0.29	0.62	0.31
		Testing	0.27	0.64	0.38	0.27	0.66	0.35	0.19	0.83	0.67
$t+5$	3	Training	0.48	0.62	0.38	0.39	0.79	0.59	0.26	0.91	0.82
		Validation	0.37	0.38	−0.17	0.32	0.45	0.16	0.29	0.61	0.29
		Testing	0.28	0.58	0.30	0.30	0.60	0.21	0.21	0.82	0.59
$t+6$	4	Training	0.48	0.64	0.38	0.43	0.71	0.50	0.26	0.91	0.82
		Validation	0.36	0.41	−0.07	0.33	0.46	0.09	0.31	0.52	0.18
		Testing	0.28	0.56	0.27	0.29	0.51	0.25	0.24	0.71	0.47

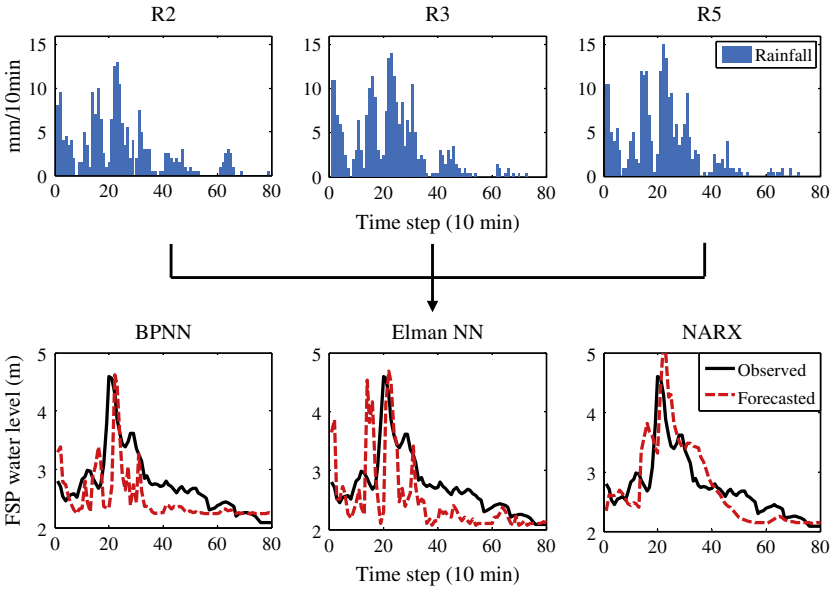

Fig. 8. Rainfall input datasets from three gauging stations and 50-min-ahead forecasts of the 612 heavy rainfall event for scenario II with respect to the BPNN, Elman NN and NARX network.

through its recursive outputs and mitigate the fluctuation problem (instability) in its output. As comparing the results obtained from scenario II, it is easy to tell that the recurrent effect from the output layer of the NARX network is more effective in modeling the long-term dependencies than the connection results from the hidden layer of the Elman NN. This result provides extra evidence that the backward connections from the hidden layer (Elman NN) could only maintain the previous values of the hidden units with an emphasis on the highly variable rainfall information. Consequently the backward connections from the hidden layer (Elman NN) impose less effects on the output than the backward connections from the output layer (NARX network), and the generalizability of the Elman NN is weaker than that of the NARX network and the BPNN.

We notice that for the NARX and the Elman NN the validation results are worse than the testing ones in all the cases of scenario II and in the $t+4$, $t+5$ and $t+6$ cases of scenario I. This is mainly because the variability of rainfall intensity (which also results in the higher variability of FSP water level) in the validation set is higher than that in the testing set (Table 1), and rainfall effect would decrease as the forecasting step exceeds the time span of rainfall affecting the rise of the FSP water level over the catchment (in our case: 40 min).

From Tables 2 and 3, we notice that all the three forecast models perform better in scenario I (w/ current FSP water level) than in scenario II (w/o current FSP water level). This reveals that the FSP water level is the dominant factor for the forecasting process. In terms of CE values produced by the NARX network in scenario II (Table 3), we notice the training cases perform equally well (0.81–0.84) for one- to six-step-ahead forecasting whereas the testing cases perform relatively poor (0.47–0.67). This is mainly because the observed input–output data (i.e., rainfall and water level) in the training stages are used to train and optimize the corresponding weights of the networks, whereas similar strategies are not implemented in the validation and testing stages.

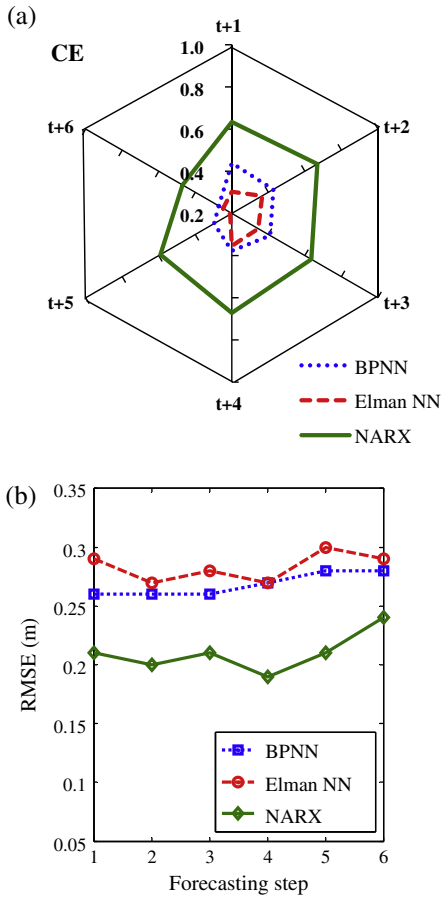

Fig. 9. (a) CE of 10- to 60-min-ahead forecasts and (b) relationship between FSP water level forecast errors (RMSE) and forecasting steps with respect to three forecast models in the testing stages for scenario II.

5. Conclusions

In this study, three ANN models (one static, two dynamic) are developed to make forecasts on the evolution of water level at floodwater storage pond (FSP) as a function of current FSP water level and rainfall information based on the inputs extracted by an advanced factor selection method (GT) for allowing sufficient time advance to warm up the pumping system and enhancing secure pumping operations to prevent the city from flooding. The temporal resolution of water level and rainfall data is 10 min, and the forecasting horizon is 60 min (i.e., 6 time steps ahead).

The results demonstrate that the GT can efficiently identify the effective rainfall factors as important inputs to the ANNs for obtain promising forecast results; and the NARX network has higher applicability than the BPNN and the Elman NN, in term of lower RMSE and higher CC and CE values for 10–60-min-ahead forecasts in both scenarios. The NARX network can well forecast the hydrograph of FSP water level and maintain the water level trail with less fluctuation, which is attributed mainly to the recurrent connections from the imperfect outputs. In addition the models constructed for scenario I (w/ current FSP water level) is superior to those of scenario II (w/o current FSP water level), which demonstrates the use of floodwater storage pond level as an input is demonstrated to improve model accuracy. Nevertheless the NARX network model for scenario II can still produce satisfactory forecasts, which suggests that the NARX network model for scenario II can be effectively implemented as an auxiliary model if current FSP water level information is not available.

In technical aspects, the outputs of the static network (BPNN) depends solely on observed data, whereas the outputs of the dynamic networks incorporate observed data with time delay units through recurrent connections and thus significant contribution could be made to the output values. The dynamic networks have the merits to effectively discover the long-term dependencies through their recursive outputs and mitigate the fluctuation problem (instability) in their outputs. Besides, the backward connections from the hidden layer (Elman NN) could only maintain the previous values of the hidden units that highly depend on the reliability of input information, and thus less effect is imposed on the output values, as compared with that of the backward connections from the output layer (NARX network).

In sum, the proposed approaches can well construct multi-step-ahead hydrological water level forecast models for urban flood control pumping. The results of this study are beneficial to the identification of inundation risks induced by inner stormwater and can be incorporated into suitable operational strategies for enhancing the pumping efficiency at inundation-prone areas.

Acknowledgements

The authors gratefully acknowledge the funding support from the Hydraulic Engineering Office, Public Works Department, Taipei City Government, Taiwan, ROC, (Grant No.: H-102-03-102124) for this research. The authors sincerely appreciate the Editor, Associate Editor and Reviewers for their valuable comments and constructive suggestions.

References

Agalbjorn, S., Koncar, N., Jones, A.J., 1997. A note on the gamma test. Neuralcomput. Appl. 5, 131–133.
Akhtar, M.K., Corzo, G.A., van Andel, S.J., Jonoski, A., 2009. River flow forecasting with artificial neural networks using satellite observed precipitation pre-processed with flow length and travel time information: case study of the Ganges river basin. Hydrol. Earth Syst. Sci. 13, 1607–1618.
Ali Ghorbani, M., Khatibi, R., Aytek, A., Makarynskyy, O., Shiri, J., 2010. Sea water level forecasting using genetic programming and comparing the performance with artificial neural networks. Comput. Geosci. 36 (5), 620–627.
Alvisi, S., Mascellani, G., Franchini, M., Bardossy, A., 2006. Water level forecasting through fuzzy logic and artificial neural network approaches. Hydro. Earth Syst. Sci. 10 (1), 1–17.
Assaad, M., Boné, R., Cardot, H., 2005. Study of the behavior of a new boosting algorithm for recurrent neural networks. Lect. Notes Comput. Sci., 169–174.
Besaw, L.E., Rizzo, D.M., Bierman, P.R., Hackett, W.R., 2010. Advances in ungauged streamflow prediction using artificial neural networks. J. Hydrol. 386 (1–4), 27–37.
Bruen, M., Yang, J.Q., 2006. Combined hydraulic and black-box models for flood forecasting in urban drainage systems. J. Hydrol. Eng. 11 (6), 589–596.
Chang, F.J., Chang, K.Y., Chang, L.C., 2008. Counterpropagation fuzzy-neural network for city flood control system. J. Hydrol. 358 (1), 24–34.
Chang, L.C., Chen, P.A., Chang, F.J., 2012. A reinforced two-step-ahead weight adjustment technique for on-line training of recurrent neural networks. IEEE Trans. Neural Network Learn. Syst. 23 (8), 1269–1278.
Chang, F.J., Chen, P.A., Liu, C.W., Liao, V.H.C., Liao, C.M., 2013. Regional estimation of groundwater arsenic concentrations through systematical dynamic-neural modeling. J. Hydrol. 499, 265–274.
Chen, P.A., Chang, L.C., Chang, F.J., 2013. Reinforced recurrent neural networks for multi-step-ahead flood forecasts. J. Hydrol. 497, 71–79.
Chiang, Y.M., Chang, L.C., Tsai, M.J., Wang, Y.F., Chang, F.J., 2010. Dynamic neural networks for real-time water level predictions of sewerage systems-covering gauged and ungauged sites. Hydrol. Earth Syst. Sci. 14 (7), 1309–1319.
Coulibaly, P., Baldwin, C.K., 2005. Nonstationary hydrological timeseries forecasting using nonlinear dynamic methods. J. Hydrol. 307 (1–4), 164–174.
Coulibaly, P., Evora, N.D., 2007. Comparison of neural network methods for infilling missing daily weather records. J. Hydrol. 341 (1–2), 27–41.
DSD, Drainage Services Department, 2000. Stormwater drainage manual – planning, design and management, third ed. Hong Kong.
Durrant, P.J., 2001. winGamma: a Non-linear Data Analysis and Modeling Tool with Applications to Flood Prediction. PhD thesis. Department of Computer Science, Cardiff University, Wales, UK.
Elman, J.L., 1990. Finding structure in time. Cognit. Sci. 14, 179–211.
Hung, N.Q., Babel, M.S., Weesakul, S., Tripathi, N.K., 2009. An artificial neural network model for rainfall forecasting in Bangkok, Thailand. Hydrol. Earth Syst. Sci. 13, 1413–1425.

Jiang, C., Song, F., 2011. Sunspot forecasting by using Chaotic time series analysis and NARX network. J. Chem. Phys. 6, 1424–1429.
Koncar, N., 1997. Optimisation methodologies for direct inverse neurocontrol. PhD thesis, Department of computing, Imperial College of Science, Technology and Medicine, University of London.
Lin, T., Horne, B.G., Giles, C.L., 1998. How embedded memory in recurrent neural network architectures helps learning long-term temporal dependencies. Neural Networks 11 (5), 861–868.
Loke, E., Warnaars, E.A., Jacobsen, P., Nelen, F., Almeida, M.D., 1997. Artificial neural networks as a tool in urban storm drainage. Water Sci. Technol. 36 (8–9), 101–109.
Ma, Q.L., Zheng, Q.L., Peng, H., Zhong, T.W., Qin, J.W., 2008. Multi-step-prediction of chaotic time series based on co-evolutionary recurrent neural network. Chin. Phys. B 17 (2), 536–542.
Maity, R., Kumar, D.N., 2008. Basin-scale stream-flow forecasting using the information of large-scale atmospheric circulation phenomena. Hydrol. Process. 22 (5), 643–650.
Makarynskyy, O., Makarynska, D., Kuhn, M., Featherstone, W.E., 2004. Predicting sea level variations with artificial neural networks at Hillarys Boat Harbour, Western Australia. Estuarine Coastal Shelf Sci. 61 (2), 351–360.
Menezes Jr., J.M.P., Barreto, G.A., 2008. Long-term time series prediction with the NARX network: an empirical evaluation. Neurocomputing 71 (16–18), 3335–3343.
Moghaddamnia, A., GhafariGousheh, M., Piri, J., Amin, S., Han, D., 2009. Evaporation estimation using artificial neural networks and adaptive neuro-fuzzy inference system techniques. Adv. Water Resour. 32, 88–97.
Muluye, G.Y., 2011. Improving long-range hydrological forecasts with extended Kalman filters. Hydrol. Sci. J. 56 (7), 1118–1128.
Nash, J.E., Sutcliffe, J.V., 1970. River flow forecasting through conceptual models: 1. A discussion of principles. J. Hydrol. 10, 282–290.
Nasseri, M., Asghari, K., Abedini, M.J., 2008. Optimized scenario for rainfall forecasting using genetic algorithm coupled with artificial neural network. Expert Syst. Appl. 35 (3), 1415–1421.
Nayak, P.C., Sudheer, K.P., Rangan, D.M., Ramasastri, K.S., 2004. A neuro-fuzzy computing technique for modeling hydrological time series. J. Hydrol. 291 (1–2), 52–66.
Nayak, P.C., Venkatesh, B., Krishna, B., Jain, S.K., 2013. Rainfall runoff modelling using conceptual, data driven and wavelet based computing approach. J. Hydrol. 493, 57–67.
Noori, R., Karbassi, A.R., Moghaddamnia, A., Han, D., Zokaei-Ashtiani, M.H., Farokhnia, A., Gousheh, M.G., 2011. Assessment of input variables determination on the SVM model performance using PCA, Gamma test, and forward selection techniques for monthly stream flow prediction. J. Hydrol. 401, 177–189.
PUB., Singapore's National Water Agency, 2013. Code of Practice on Surface Water Drainage, sixth ed. Singapore.
Rumelhart, D.E., Hinton, G.E., Williams, R.J., 1986. Learning representations by back-propagating errors. Nature 323 (6088), 533–536.
Sahoo, G.B., Schladow, S.G., Reuter, J.E., 2009. Forecasting stream water temperature using regression analysis, artificial neural network, and chaotic non-linear dynamic models. J. Hydrol. 378 (3–4), 25–342.
Serpen, G., Xu, Y., 2003. Simultaneous recurrent neural network trained with non-recurrent backpropagation algorithm for static optimisation. Neural Comput. Appl. 12, 1–9.
Shen, H.Y., Chang, L.C., 2013. Online multistep-ahead inundation depth forecasts by recurrent NARX networks. Hydrol. Earth Syst. Sci. 17 (3), 935–945.
Sorjamaa, A., Hao, J., Reyhani, N., Ji, Y., Lendasse, A., 2007. Methodology for long-term prediction of time series. Neurocomputing 70 (16–18), 2861–2869.
Sudheer, K.P., Srinivasan, K., Neelakantan, T.R., Srinivas, V.V., 2008. A nonlinear data-driven model for synthetic generation of annual streamflows. Hydrol. Process. 22 (12), 1831–1845.
Tamoto, N., Endo, J., Yoshimoto, K., Yoshida, T., Sakakibara, T., 2008. Forecast-based operation method in minimizing flood damage in urban area. Int. Conf. Urban Drain. 11th, Edinburgh, Scotland, UK.
Toth, E., 2009. Classification of hydro-meteorological conditions and multiple artificial neural networks for streamflow forecasting. Hydrol. Earth Syst. Sci. 13, 1555–1566.
Tsui, A.P.M., Jones, A.J., Guedes de Oliveira, A.G., 2002. The construction of smooth models using irregular embeddings determined by a gamma test analysis. Neural Comput. Appl. 10 (4), 318–329.